Int. J. Solids Structures Vol. 14, pp. 821–839

0020-7683/78/1001-0821/$02.00/0

ACTIVE FEEDBACK CONTROL OF A BEAM SUBJECTED TO A NONCONSERVATIVE FORCE

HIDETSUGU HORIKAWA
Assistant-in-Research, Department of Aerospace and Mechanical Sciences, Princeton University, Princeton, NJ 08540, U.S.A.

EARL H. DOWELL
Professor, Department of Aerospace and Mechanical Sciences, Princeton University, Princeton, NJ 08540, U.S.A.

and

FRANCIS C. MOON
Associate Professor, Department of Theoretical and Applied Mechanics, Cornell University, Ithaca, NY 14850, U.S.A.

(*Received* 31 *August* 1977; *in revised form* 5 *January* 1978; *received for publication* 15 *February* 1978)

Abstract—This study examines the possibility of controlling through feedback a thin cantilevered beam subjected to a nonconservative follower force. A converging frequency flutter instability which occurs in this model is similar to classical bending-torsion flutter of an aircraft wing. Because of the similar nature of the instabilities, the beam under the follower force can be a useful vehicle for investigating the fundamental aspects of stabilization of wing flutter by feedback control. A modal approach is used for obtaining the mathematical model and control laws. A standard root locus technique for simple analytical models is also used to understand and explain the control of the beam. Experiments are carried out to verify the validity of this theoretical model. Good correlation is shown between theoretically and experimentally determined stability boundaries as well as for modal frequency and damping variation with follower force.

NOTATION

A_m	bending mode coefficients
$a_m = A_{m/L}$	nondimensional bending mode coefficients
B_r	torsion mode coefficients
C	modal integrals
E	Young modulus
F_r	torsion modal constant, $F_r^2 \equiv mr^2\omega_r^2L^2/GJ$
G_m	bending modal constant, $G_m^4 \equiv m\omega_m^2L^4/EI$
G	shear modulus
h	beam thickness
I	bending moment of inertia
J	torsion moment of inertia
K_m	non-dimensional frequency $\equiv (m\omega^2L^4/EI)^{1/2} \equiv G_m^2$
k_s	non-dimensional torsion strain feedback gain = V_sLh/EI
k_v	non-dimensional torsion velocity feedback gain = $V_v/(mEI)^{1/2}$
k_a	non-dimensional torsion acceleration feedback gain = V_a/mL^2
L	beam length
$\mathbf{M}$	moment vector
m	beam density
Q	control force
$\mathbf{q}$	body force
r	beam radius of gyration
r_c	perpendicular distance from elastic axis to control force
s	Laplace transform variable
t	time
u	bending displacement
u_n	bending natural mode
V^0	follower force (tip jet force)
V	feedback loop transfer function
$\mathbf{V}$	shear force vector
x, y, z	coordinate system of undeformed beam
x', y', z'	coordinate system of deformed beam
z_c	position of control force
z_s	position of strain gage
z_a	position of accelerometer
γ	torsion/bending stiffness ratio = GJ/EI, also torsion strain
λ	non-dimensional follower force = V^0L^2/EI

ϕ torsion displacement
ϕ_s torsion natural mode
ρ non-dimensional radius of gyration = r/L
ρ_c non-dimensional control force moment arm = r_c/L
τ non-dimensional time = $(EIt^2/mL^4)^{1/2}$, also body torque
ω frequency
Ω_m non-dimensional torsion frequency = $(\gamma F_m^2/\rho^2)^{1/2}$

Superscript
0 initial load
' $\partial/\partial(z/L)$

Subscript
F flutter
D divergence
d displacement
s strain
v velocity
a acceleration

1. INTRODUCTION

It is well known that a dynamic instability (flutter) may be induced in elastic systems under a non-conservative force[1–13]. As one of these problems, wing flutter on an airplane is extremely important. The prevention of wing flutter by utilizing a controllable force which responds to feedback signals from motion sensors located on the main lifting surface has received recent attention. Most of these studies[1, 2] began late in the 1960s and the subject is still rapidly developing[3]. Many of the earlier studies, however, are of an *ad hoc* nature and it has been difficult to assess the meaning and generality of the results obtained.

A simple experimental model with a non-conservative force has been proposed[4–8] in order to gain insight into the fundamentals of flutter suppression systems. The experiment consists of a thin cantilevered beam with an air nozzle mounted at its tip parallel to the chord line (Fig. 1). Not only does this model resemble a thin wing with tip jet, but it also experiences a converging frequency flutter instability similar to a classical bending-torsion wing flutter. This similarity, along with the simplicity and flexibility of the experiment compared with a wind tunnel flutter experiment, gives it a potential use as a prototype for investigating the effect of feedback control in suppressing flutter of more complex systems.

Dowell and Moon[4] conducted one of the first investigations of this type of flutter instability in a continuous elastic system. Prasad and Herrmann[9] had investigated this instability previously without feedback control. The purpose of the study in [4] was to attempt to suppress or delay the start of an instability in a non-conservative mechanical system using feedback control. The configuration studied was a torsion strain signal feedback. They concluded that for flutter instability of a beam under a jet follower force *without feedback*

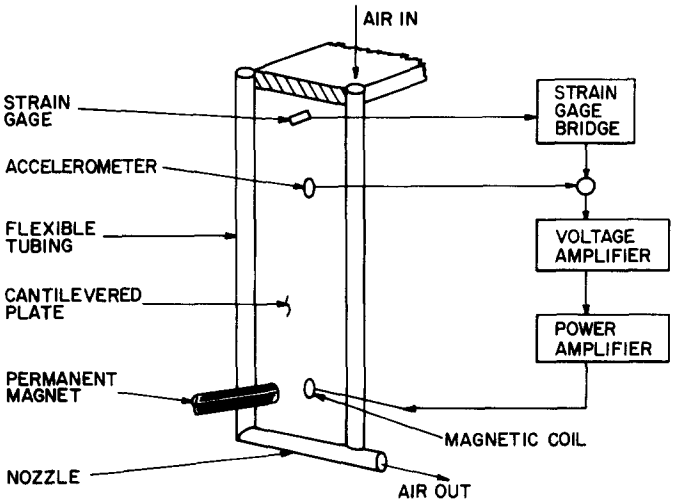

Fig. 1. Schematic of system.

control there is a good correlation between theory and experiment. However, the omission of a term in the non-dimensional form of the control equation presented in [4] resulted in the prediction of an incorrect stability boundary. Dowell, Moon and Kalmbach later added this missing term to the theoretical analysis and constructed a more sophisticated experiment [5–7]. These improvements indicated that substantial suppression of flutter could be achieved using only pure gain compensation of a torsion strain signal. At this stage, the feedback loop configuration consisted of a static type torsion strain signal. Dynamic feedback signals, such as velocity or acceleration, have been studied more recently [8]. Generally speaking, only a few systematic studies of feedback systems for flutter suppression can be found in the literature [3, 15].

The scope of the current research accomplished beyond that described in [7] encompasses systematic theoretical and experimental studies of the effects on flutter of various control systems including strain, velocity, and/or acceleration signal feedbacks. The direct purpose is two-fold. Firstly, the study of a dynamic feedback signal, i.e. torsion velocity and acceleration, will be done. The effect of the torsion acceleration feedback loop, which is added to the torsion strain feedback link, on the stability boundary is emphasized. Secondly the behavior of the beam model below the flutter boundary will be explored. Several techniques without external excitations have been applied to obtain the subcritical response [3] for a wing using the natural turbulence in a wind tunnel. In this model, however, the beam itself is not in an air flow. Therefore the well-known forced response method was used and satisfactory data were recorded.

2. THEORETICAL MODEL AND APPLICATION OF STANDARD ROOT LOCUS METHOD TO SIMPLE SYSTEMS

Referring to a differential element of the beam (Fig. 2), the equations for a cantilevered thin beam are obtained as follows [7, 8],

$$m\frac{\partial^2 u}{\partial t^2}+EI\frac{\partial^2 u}{\partial z^4}+2V_y^0\frac{\partial \phi}{\partial z}+M_x^0\frac{\partial^2 \phi}{\partial z^2}=q_x \tag{1a}$$

$$mr^2\frac{\partial^2 \phi}{\partial t^2}-GJ\frac{\partial^2 \phi}{\partial z^2}+M_x^0\frac{\partial^2 u}{\partial z^2}=\tau_z. \tag{1b}$$

Boundary conditions for this case are

$$u=\frac{\partial u}{\partial z}=\phi=0 \qquad \text{at} \quad z=0$$

$$\frac{\partial^2 u}{\partial z^2}=\frac{\partial^3 u}{\partial z^3}=\frac{\partial \phi}{\partial z}=0 \qquad \text{at} \quad z=L. \tag{2}$$

The basic assumptions underlying eqns (1) are

- Beam model (chord line is rigid).
- The beam is initially stressed in the chordwise direction.
- Displacements u and ϕ are small.
- The rotational intertia about the y-axis is neglected.
- Hooke's law.

Equations (1) are variable coefficient, partial differential equations. These are reduced to constant coefficient, ordinary differential equations via Galerkin's method for stability analysis.

Let u_m and ϕ_r be natural modes in bending and torsion of a clamped-free beam and assume

$$u=\sum_m A_m(t)u_m(z)$$

$$\phi=\sum_r B_r(t)\phi_r(z). \tag{3}$$

The functions u_m and ϕ_r satisfy the boundary conditions (2) as well as the following differential

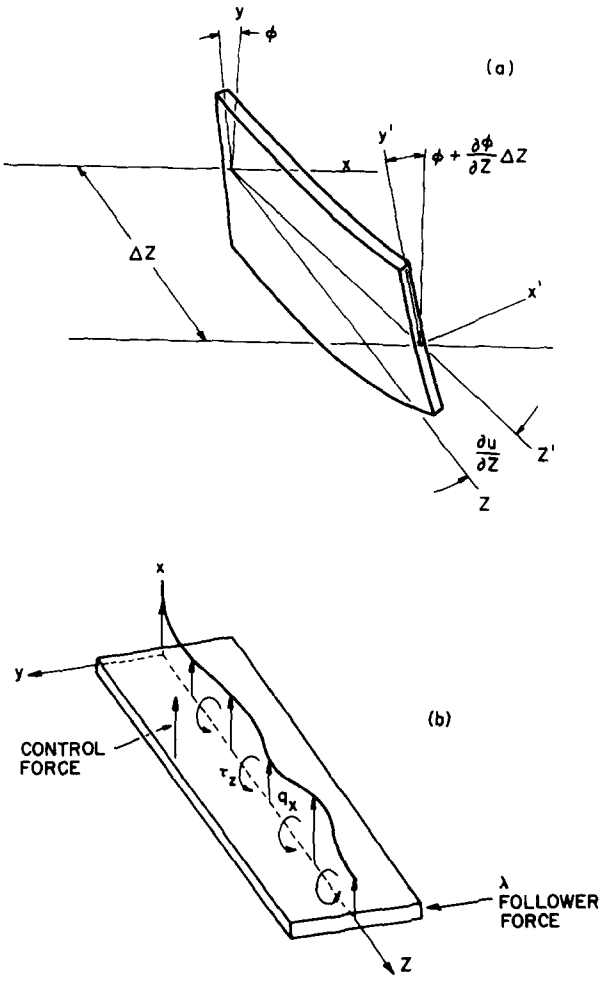

Fig. 2. Coordinate system.

equations, in which G_m and F_r are known constants [$' \equiv (\partial/\partial(z/L))$]:

$$u_m''' - G_m^4 u_m = 0$$
$$\phi_r'' + F_r^2 \phi_r = 0. \tag{4}$$

The following equations are obtained after substituting (3) into (1), observing (4), multiplying (1a) by u_n and (1b) by ϕ_s, and finally integrating over z.

$$\left(m\frac{\partial^2 A_n}{\partial t^2} + \frac{EI}{L^4} G_n^4 A_n\right) \int_0^1 u_n^2 \, \mathrm{d}\left(\frac{z}{L}\right) + \frac{2}{L} \sum_r B_r \int_0^1 V_y^0 \phi_r' u_n \, \mathrm{d}\left(\frac{z}{L}\right)$$
$$+ \frac{1}{L^2} \sum_r B_r \int_0^1 M_x^0 \phi_r'' u_n \, \mathrm{d}\left(\frac{z}{L}\right) = \int_0^1 q_x u_n \, \mathrm{d}\left(\frac{z}{L}\right)$$
$$\left(mr^2 \frac{\mathrm{d}^2 B_s}{\mathrm{d}t^2} + \frac{GJ}{L^2} F_s^2 B_s\right) \int_0^1 \phi_s^2 \, \mathrm{d}\left(\frac{z}{L}\right) + \frac{1}{L^2} \sum_m A_m \int_0^1 M_x^0 u_m'' \phi_s \, \mathrm{d}\left(\frac{z}{L}\right)$$
$$= \int_0^1 \tau_z \phi_s \, \mathrm{d}\left(\frac{z}{L}\right). \tag{5}$$

Follower and control forces must be specified to model the experimental configuration studied. First, the follower force is located at the tip of the beam, so

$$V_y^0 = V^0, \quad M_x^0 = V^0(z - L). \tag{6}$$

The control force, Q, which is assumed as a point force, depends on feedback laws. Thus

$$q_x = Q\delta(z - z_c), \quad \tau_z = -r_c Q\delta(z - z_c) \tag{7a}$$

where

$$Q = V_s\gamma(z_s) = V_s . 2\frac{h}{L}\phi'(z_s) \qquad \text{(torsion strain feedback)}$$

or

$$= V_v\dot{\phi}(z_v) \qquad \text{(torsion velocity feedback)} \tag{7b}$$

or

$$= V_a\ddot{\phi}(z_a). \qquad \text{(torsion acceleration feedback).}$$

Substituting (6) and (7) into (5) and non-dimensionalizing as noted in the Notation, one obtains

$$\left(\frac{d^2a_n}{d\tau^2} + K_n^2 a_n\right) C1_{nn} + \lambda \sum_r B_r C8_{rn}$$

$$= k_s u_n(z_c) \sum_r B_r \phi_r'(z_s) \qquad \text{(strain feedback)}$$

$$= k_v u_n(z_c) \sum_r \frac{dB_r}{d\tau} \phi_r(z_v) \qquad \text{(velocity feedback)}$$

$$= k_a u_n(z_c) \sum_r \frac{d^2B}{d\tau^2} \phi_r(z_a) \qquad \text{(acceleration feedback)} \tag{8}$$

$$\left(\frac{d^2B_s}{d\tau^2} + \Omega_s^2 B_s\right) C2_{ss} + \frac{\lambda}{\rho^2} \sum_m a_m C9_{sm}$$

$$= k_s \frac{\rho_c}{\rho^2} \phi_s(z_c) \sum_r B_r \phi_r'(z_s) \qquad \text{(strain feedback)}$$

$$= k_v \frac{\rho_c}{\rho^2} \phi_s(z_c) \sum_r \frac{dB_r}{d\tau} \phi_r(z_v) \qquad \text{(velocity feedback)}$$

$$= -k_a \frac{\rho_c}{\rho^2} \phi_s(z_c) \sum_r \frac{d^2B_r}{d\tau^2} \phi_r(z_a) \qquad \text{(acceleration feedback)}$$

where the modal integrals C1, C2, C8 and C9 are defined in Ref. [8]. When structural damping is included of the viscous type, the terms $2\zeta_n K_n(da_n/d\tau)$ and $2\zeta_s\Omega_s(dB_s/d\tau)$ are added into the parentheses on the l.h.s. of (8).

Equations (8) are now a system of ordinary differential equations for the $a_n(= A_n/L)$ and B_s, the coefficients of the natural modes defined in (3). The characteristic determinant of the Laplace transformed equations shown above is used for the dynamic stability analysis of this problem. If one of the real parts of the characteristic roots becomes positive, diverging unstable motions occur for the system.

Before presenting numerical and experimental studies for specific cases, a graphical root locus technique is employed to select promising model configurations and parameter variations. This classical standard root locus method is applicable when a three mode, no structural damping model is assumed since the characteristic equation can be reduced to the $1 + KG = 0$ form and higher powers of K do not appear. The three modes retained are the first two bending and lowest torsion. The characteristic equation for torsion strain feedback system is

$$\Delta = C1_{11}C1_{22}C2_{11}(s^2 + K_1^2)(s^2 + K_2^2)(s^2 + \Omega_1^2) - \frac{\lambda^2}{\rho^2}\{C8_{11}C9_{11}C1_{22}(s^2 + K_2^2)$$

$$+ C8_{12}C9_{12}C1_{11}(s^2 + K_1^2)\} + k_s \frac{\phi_1'(z_s)}{\rho^2}[\rho_c C1_{11}C1_{22}\phi_1(z_c)(s^2 + K_1^2)(s^2 + K_2^2)$$

$$+ \lambda\{C9_{11}C1_{22}u_1(z_c)(s^2 + K_2^2) + C9_{12}C1_{11}u_2(z_c)(s^2 + K_1^2)\}]$$

$$= \Delta_{\text{beam, jet}}(s, \lambda^2) + k_s\Delta_{\text{control}}(s, \lambda) = 0. \tag{9}$$

The present problem can be cast into an equivalent root locus form[14]. Thus the hypothetical open-loop transfer function for (9) is

$$G = k_s C \frac{N(s^2, \lambda)}{D(s^2, \lambda^2)} \tag{10}$$

where k_s: nondimensional torsion strain feedback gain

$$C = \frac{\phi_1'(z_s)}{\rho^2} \frac{\rho_c \phi_1(z_c)}{C2_{11}} = \text{constant}$$

$$D(s, \lambda^2) = (s^2 + K_1^2)(s^2 + K_2^2)(s^2 + \Omega_1^2) - \lambda^2 \frac{C8_{11}C9_{11}C1_{22}(s^2 + K_2^2) + C8_{12}C9_{12}C1_{11}(s^2 + K_1^2)}{\rho^2 C1_{11}C1_{22}C2_{11}}$$

$$N(s, \lambda) = (s^2 + K_1^2)(s^2 + K_2^2) + \lambda \frac{C9_{11}C1_{22}u_1(z_c)(s^2 + K_2^2) + C9_{12}C1_{11}u_2(z_c)(s^2 + K_1^2)}{\rho_c C1_{11}C1_{22}\phi_1(z_c)}.$$

As may be seen, the poles and zeros of the open loop transfer function depend upon the follower force λ. By examining these movements and locating them on the s-plane for a certain λ, one can study the influence of k_s to this system.

First, the denominator is the characteristic equation for the beam-follower force system without feedback control. One can check the roots of D by reducing this to the root locus form again

$$1 + G_d = 1 + \lambda^2 C_d \frac{N_d}{D_d} = 1 + \lambda^2 C_d \frac{s^2 + A_d}{(s^2 + K_1^2)(s^2 + K_2^2)(s^2 + \Omega_1^2)} = 0 \tag{11}$$

where

$$C_d = -\frac{C8_{11}C9_{11}C1_{22} + C8_{12}C9_{12}C1_{11}}{C1_{11}C1_{22}C2_{11}}$$

$$A_d = \frac{C8_{11}C9_{11}C1_{22}K_2^2 + C8_{12}C9_{12}C1_{11}K_1^2}{C8_{11}C9_{11}C1_{22} + C8_{12}C9_{12}C1_{11}}.$$

In the same way as for D, the roots of N can be obtained in the following root locus;

$$1 + G_n = 1 + \lambda C_n \frac{N_n}{D_n} = 1 + \lambda C_n \frac{s^2 + A_n}{(s^2 + K_1^2)(s^2 + K_2^2)} = 0 \tag{12}$$

where

$$C_n = \frac{C9_{11}C1_{22}u_1(z_c) + C9_{12}C1_{11}u_2(z_c)}{\rho_c C1_{11}C1_{22}\phi_1(z_c)}$$

$$A_n = \frac{C9_{11}C1_{22}u_1(z_c)K_2^2 + C9_{12}C1_{11}u_2(z_c)K_1^2}{C9_{11}C1_{22}u_1(z_c) + C9_{12}C1_{11}u_2(z_c)}.$$

Once the poles and zeros of (10) for some λ_{fixed} are obtained, the required solutions of (9) are derived by applying the root locus procedure to the problem for G.

The above method is applied to two specific cases, that is, the control force locations $z_{c/L} = 0.3$ and 0.9. $z_{c/L} = 0.9$ was chosen because it represents the best intuitive choice† for control placement. $z_{c/L} = 0.3$ was chosen because at this station the greatest stable variation of k_s at high λ was recorded in[6, 7].

Figure 3, where $z_{c/L} = 0.3$, shows system pole and zero migrations for the follower force variation. This model with no control force goes into flutter at $\lambda = 13.9$. In order to examine the

†It is intuitive in the sense that the first bending and torsion modes exhibit their maximum displacements near the tip of the beam.

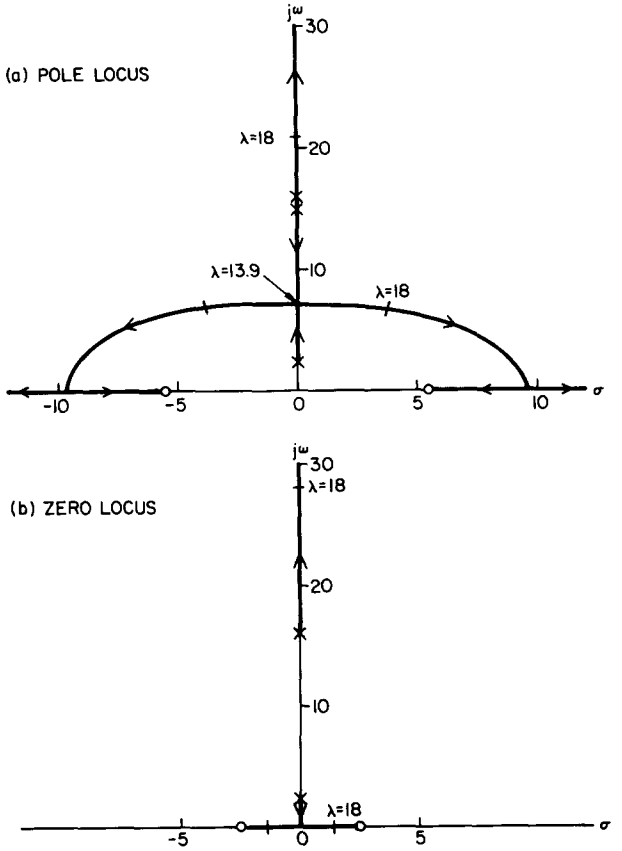

Fig. 3. Pole and zero loci for G_d and $G_n(z_{c/L} = 0.3)$.

effect of the feedback loop, a certain unstable condition is selected, say $\lambda = 18.0$. Once the locations of poles and zeros for $\lambda = 18.0$ are specified in Fig. 3, the root locus for the total system with torsion strain feedback is obtained as shown in Fig. 4. This system recovers stability at $k_s = 8.5$. As the feedback gain k_s is increased further, one of the stabilized branches is merged with the third mode branch and loses stability again at $k_s = 21.4$ in the form of flutter with a higher frequency. The other stabilized branch undergoes divergence at $k_s = 250$.

As the next step, a first order lead compensation is considered, which means the addition of a velocity feedback. In this case one can easily conclude that there is no way of stabilizing the fluttering roots. Since N/D in (10) is always a real number for any value on the imaginary axis in this system without structural or aerodynamic damping, it is impossible for odd order compensation to satisfy the 180° angle condition for the root locus on the imaginary axis except at the origin. Even if two unstable roots merge together on the positive real axis and one of them enters into the stable left half plane through the origin, the other branch stays in the right half plane. This means that unstable roots can never return to the left half plane or imaginary axis in the s-plane. The introduction of velocity feedback does not work at all in this particular system. A root locus example using pure velocity feedback of torsion strain is shown in Fig. 5.

Careful inspection of Fig. 4 suggests one interesting feedback compensation. If zeros are placed between the point where the unstable root comes back to the imaginary axis and the highest frequency pole, the higher frequency flutter can be perfectly suppressed in this three mode analysis. This compensation is a combination of strain and its acceleration. A root locus plot is shown in Fig. 6.

The other control force location studied is $z_{c/L} = 0.9$. Figure 7 shows system pole and zero migrations for the follower force variation. The pole locus in Fig. 7(a) is essentially the same as that in Fig. 3(a). The change of the wire coils' weight location results in a slight pole locus difference between them.† The zero locus in Fig. 7(b), however, is quite different from Fig. 3(b).

†See discussion of experimental apparatus in following section.

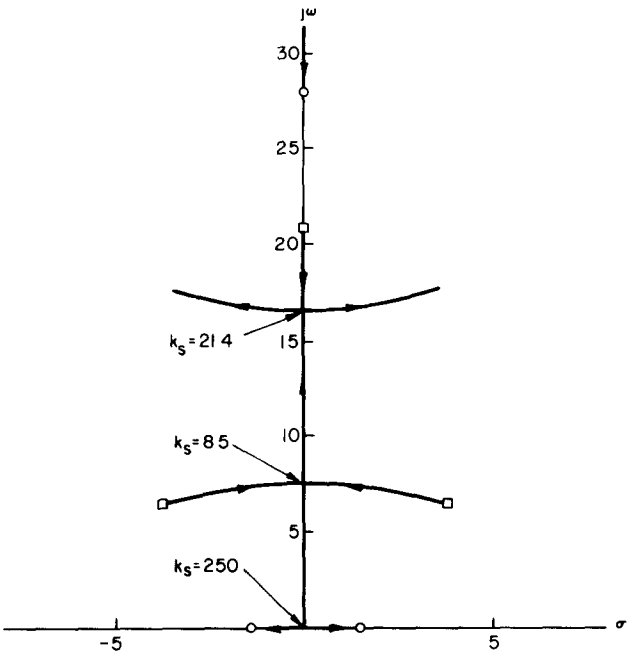

Fig. 4. Root locus for $G(s, \lambda = 18)$ ($z_{c/L} = 0.3$).

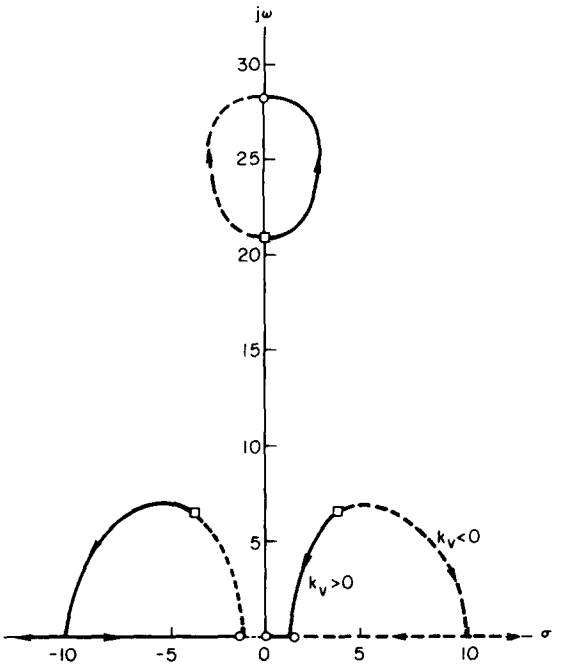

Fig. 5. Root locus for $sG(s, \lambda = 18)$ ($z_{c/L} = 0.3$).

Figure 8 is the system root locus for k_s at $\lambda = 18.0$. The unstable root is stabilized at $k_s = 5.9$ and goes into a divergence instability at $k_s = 10.6$ instead of high frequency flutter. This difference between Figs. 4 and 8 clearly comes from zero locations. The zero on the imaginary axis in Fig. 4 is above the pole and the zeros on the real axis are much closer to the origin in Fig. 4. This reversal of the pole and zero locations on the imaginary axis in Fig. 8 brings no possibility of high frequency flutter. By contrast, divergence in Fig. 8 is induced rather easily due to zero locations on the real axis far away from origin. Velocity feedback does not work for

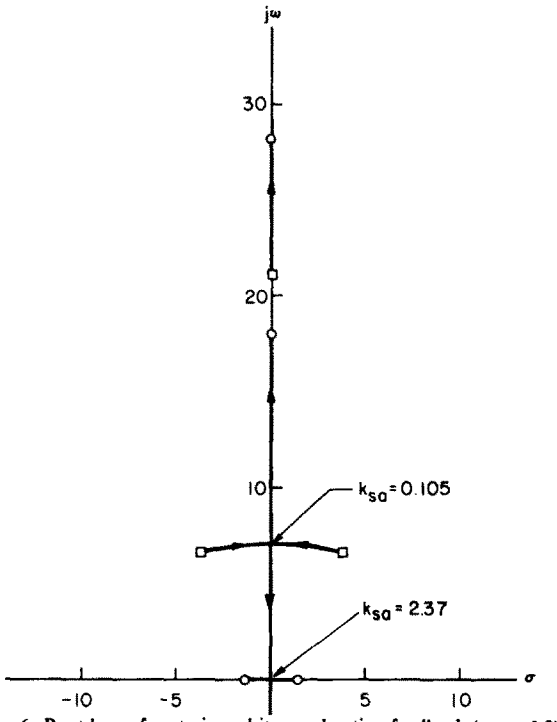

Fig. 6. Root locus for strain and its acceleration feedback ($z_{c/L} = 0.3$).

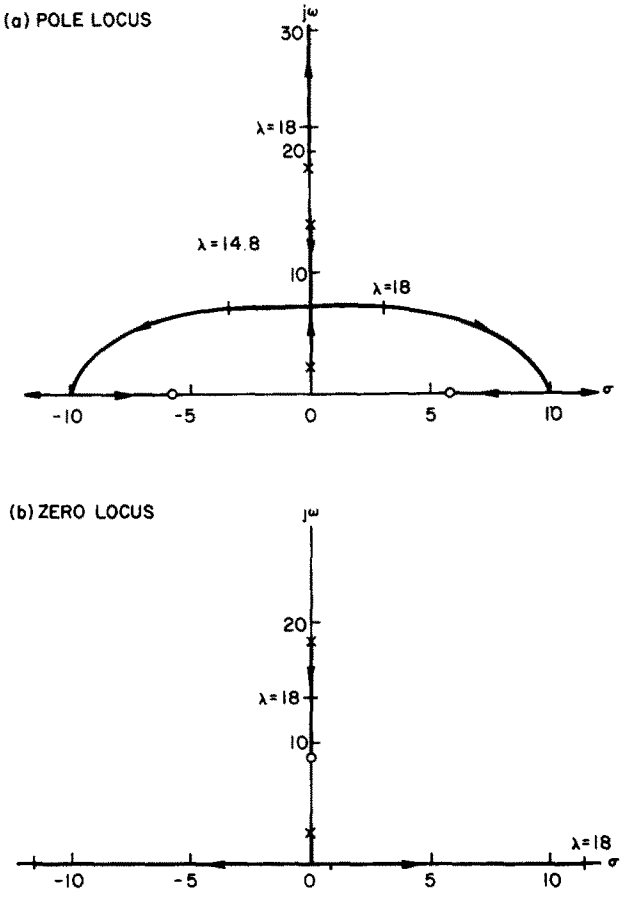

Fig. 7. Pole and zero loci for G_d and $G_n(z_{c/L} = 0.9)$.

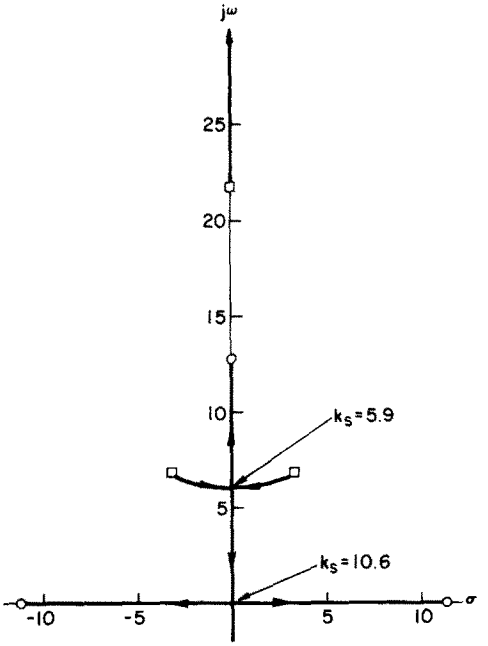

Fig. 8. Root locus for $G(s, \lambda = 18)$ ($z_{c/L} = 0.9$).

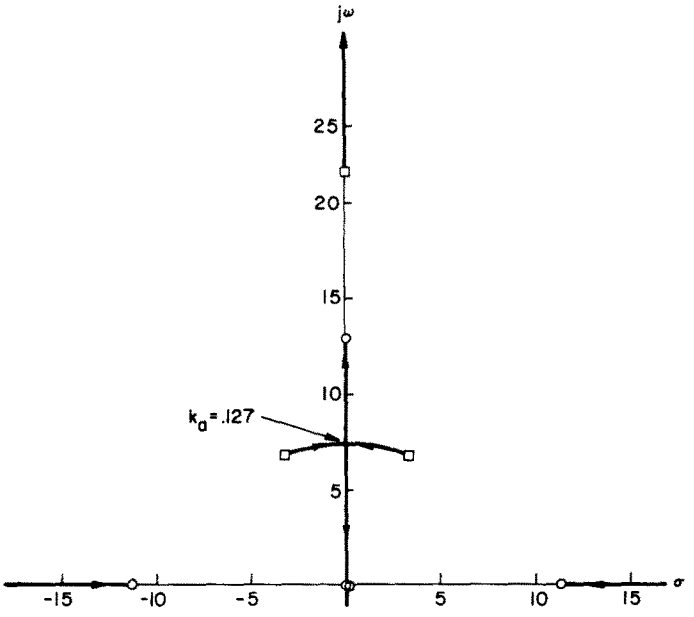

Fig. 9. Root locus for $s^2G(s, \lambda = 18)$ ($z_{c/L} = 0.9$).

the same reason discussed earlier. Even acceleration feedback is not beneficial in this configuration since zeros on the real axis easily induce divergence at infinity (Fig. 9).

As long as only a first torsion mode is assumed in the numerical analysis, torsion strain and displacement are equivalent because they are both in the same phase along the span, and are connected by a proportional relation. If more than two torsion modes are assumed in the analysis, this simple relation between them fails in general.

3. NUMERICAL AND EXPERIMENTAL STUDIES

As a result of root locus analysis, it is known that the introduction of acceleration feedback in addition to strain signal may suppress or delay the high frequency flutter at the control force location $z_{c/L} = 0.3$. The studies in this section investigate this configuration in more depth.

3.1 *Computer model*

The computer programs used are described in detail in [8]. Figure 10 is an example of stability boundaries, which show the effect of the number of assumed modes and structural damping. A change from a diagonal to a full mass matrix introduced in the current theoretical model permits prediction of the divergence boundary which was missed in the earlier theoretical analysis[6, 7]. That is, in the present analysis full mass coupling due to localized masses of tubes, accelerometers, etc. is accounted for with the stiffness inferred from measured natural frequencies[8]. A convergence study using various numbers of modes showed that a nine mode model is required for accurate determination of the divergence boundary. Inclusion of structural damping is also important for the prediction of the low frequency flutter boundary. A nine mode, structural damping model would give better accuracy than those in Fig. 10, but it takes an enormous amount of calculation time.

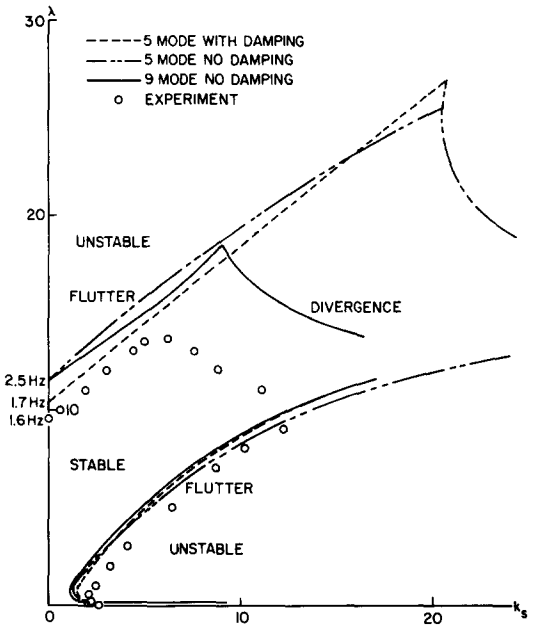

Fig. 10. Damping effect on stability boundary ($z_{c/L} = 0.9$).

For the sake of consistency, all theoretical curves for stability boundaries are the products of the nine mode, no structural damping model. A five mode, structural damping model is employed for frequency and damping variation with follower and control forces in Section 3.3.2.

3.2 *Experimental apparatus*

The details of the experimental apparatus are discussed in [7, 8]. Figure 11 is a picture of a beam specimen. Strain gages are mounted near the root of the beam and wire coils and accelerometers near the tip. To preserve mass and stiffness symmetry about the mid-chord axis two tubes, two pairs of wire coils, etc. are used. On both sides of the second (active) pair of coils are cylindrical permanent magnets clamped to a retort stand. The output of the torsion strain gage bridge and/or accelerometers is connected to the wire coils on the beam through electronic amplifiers, one an operational signal amplifier and the other a bipolar power amplifier.† Attached to the tip of the beam is the nozzle which is connected to two pieces of plastic tubing. The left hand tube delivers the air to the nozzle from an air compressor.

Two linear accelerometers were employed to obtain a torsional acceleration of the beam motion. Each was placed on the opposite side of the plate at the same spanwise location. The arm length of the accelerometers from the midchord line is the same as that for the wire coils. Two acceleration signals from both sides of the plate are added together, which cancels the

†A band pass filter to avoid d.c. drift is also employed which is the limiting factor on the electronic performance of the system. Measurable phase shift is present above 10 cps; no gain degradation is observed, however[8].

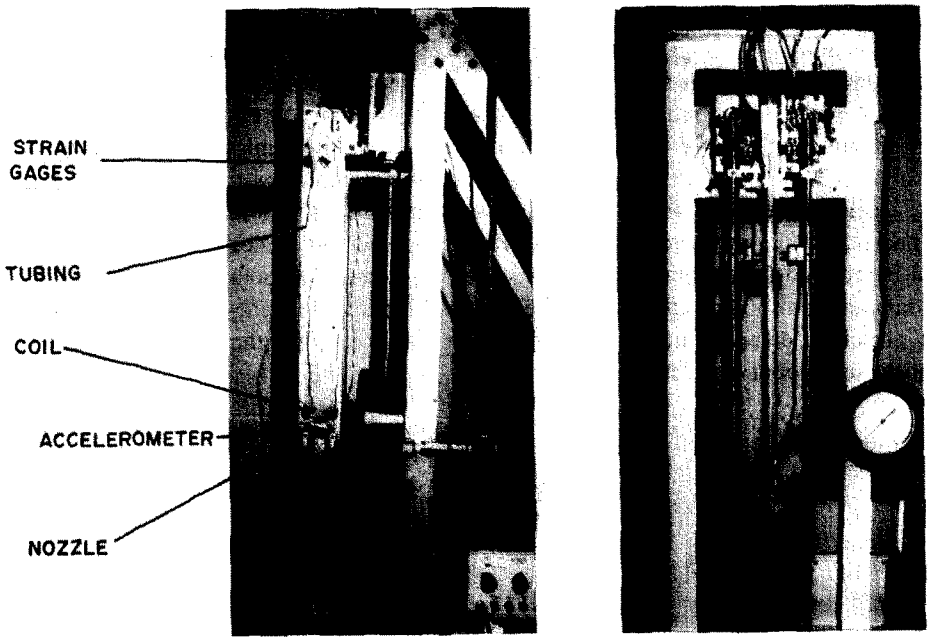

Fig. 11. Experimental apparatus.

pure bending acceleration component of the beam motion and extracts the pure torsion acceleration component. A torsion velocity feedback signal is obtained by integrating the torsion acceleration signal from the accelerometers on the beam.

3.3 *Correlation of numerical results and experiment*

3.3.1 *Stability boundaries.* The merit of a control system configuration can be determined with the aid of jet force, λ, vs active feedback gain, k, stability curves. Close agreement between the theoretical predictions and actual observations indicates a good understanding of the manner in which the application of feedback control affects the system stability boundary.

(a) *Torsion acceleration and strain feedback*

Figure 12 shows both the experimentally and theoretically obtained stability boundaries for the control force location $z_{c/L} = 0.3$ and the accelerometer location $z_{a/L} = 0.95$. λ is a nondimensional follower force parameter, k_s is a torsion strain feedback gain, and k_a is a torsion acceleration feedback gain. Figure 12(a), where k_a is zero, has been studied in [5–7]. Figure 12(b) presents the effect of k_a. Correlations between theory and experiment in these figures show reasonable agreement. Especially the effect of the torsion acceleration feedback on the torsion strain feedback configuration is well confirmed. There exists a $5 \sim 35\%$ difference between theory and experiment for the low frequency flutter boundary. Theory is always non-conservative for this boundary. This is attributed mainly to the neglect of the structural damping effect. It is known that the inclusion of the structural damping is destabilizing[8, 10, 11], that is to say, lowers the theoretical flutter boundary for this non-conservative system. If even the five mody model including structural damping effect is employed for the theoretical boundary, the gap between theory and experiment can be narrowed (Fig. 10). The descrepancies for the divergence boundary possibly come from the sluggish convergence of this portion of the theoretical boundary with increasing number of assumed modes (Fig. 10). Other possible causes of the error are discussed in Ref. [8].

The control system is evaluated not only by the achievement of the highest stability boundary, but also by the stability area. In other words, the system which gives rise to simple stability boundaries is superior to that with complex stability boundaries even if the highest stability boundaries are the same[12]. For example and by contrast, in the system in Fig. 12(a), the feedback gain must be adapted to obtain its highest stability boundary. Instability is induced by increasing the follower force when the gain is not programmed to reach the peak of the stability boundary from the zero follower force condition. If the torsion acceleration signal as

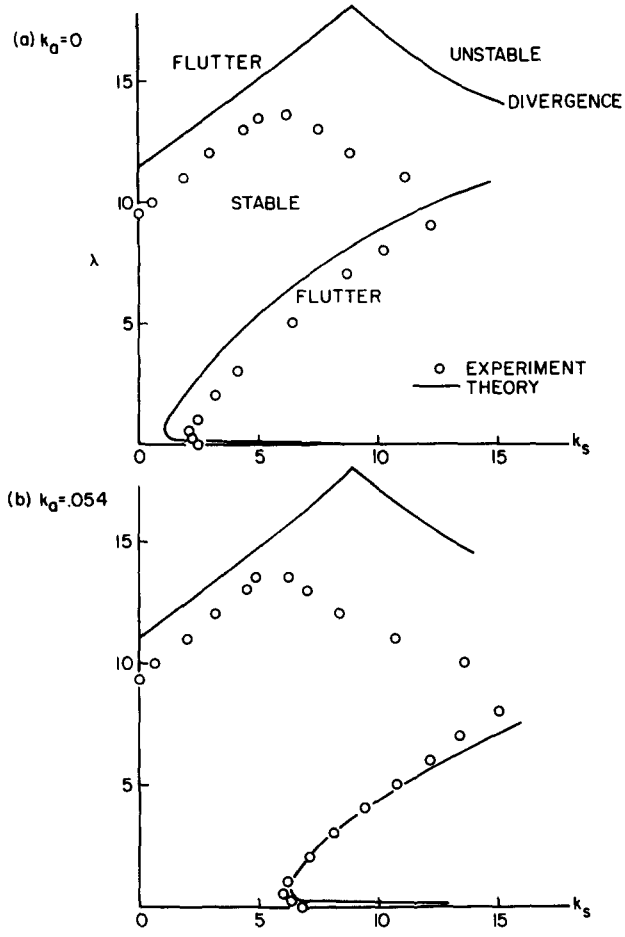

Fig. 12. Stability boundary ($z_{c/L} = 0.3$, $z_{a/L} = 0.95$).

well as strain signal is concurrently fed back as in Fig. 12(b), this unfavorable high frequency flutter region is pushed to the right and the stable area is widen. In Fig. 12(b), there is no unstable region beneath the highest stability point for the experimental results and hence no need for gain programming to reach this point.

The merit of the addition of the acceleration feedback loop is shown impressively by a time response of the system. Figure 13(a) shows the measured time response of the configuration with torsion strain feedback only. Although the torsion strain $k_s = 3$ suppresses the low frequency flutter at $\lambda = 11.0$, the same amount of increase in k_s at $\lambda = 1.0$ induces a violent high frequency flutter phenomena into the initially stable system. When the acceleration feedback loop is also closed at the same time (Fig. 13b), the high frequency flutter is perfectly suppressed while no serious changes in the low frequency flutter suppression are evident.

The low frequency flutter and divergence boundaries are less sensitive to the addition of the torsion acceleration feedback link. Theoretically, divergence must be insensitive to this feedback. If this discussion is extended to the case for the control force location $z_{c/L} = 0.9$, where stability boundaries consist of only low frequency flutter and divergence, one cannot expect great improvement of the system by the addition of acceleration feedback. Figure 14 confirms this expectation. Experimental error may have caused the slight difference among divergence boundaries when k_a is changed. For these stability boundaries at $z_{c/L} = 0.9$, the acceleration feedback addition brings no fruitful results.

(b) *Torsion acceleration feedback*

Figure 15 is an example of stability boundaries for pure torsion acceleration feedback. The system is stable under or within the curve. All the stability boundaries are flutter phenomena. Since the acceleration feedback does not modify the constant term of the characteristic polynomials, divergence does not take place by the addition of k_a unless the stability boundary

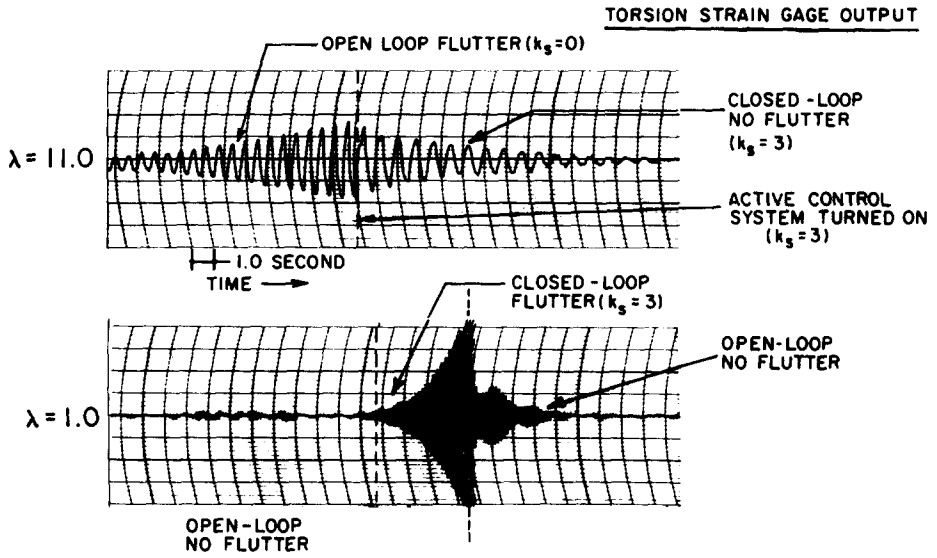

(a) ACCELERATION FEEDBACK LOOP OPEN (PHASE 2, k_a=0)

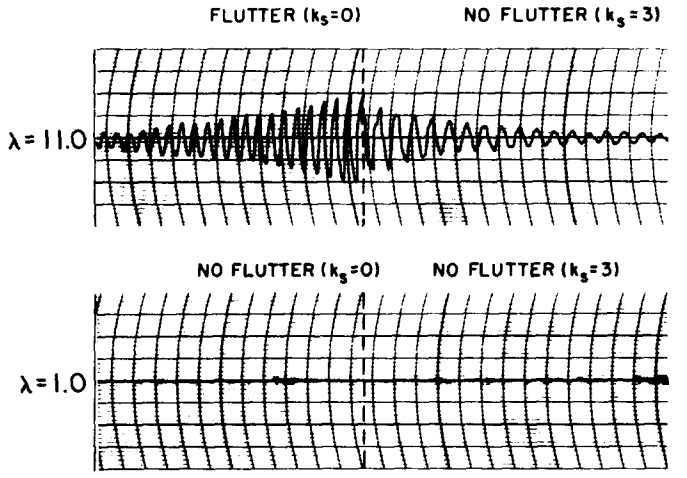

(b) ACCELERATION FEEDBACK LOOP CLOSED (PHASE 3, k_a=0.054)

Fig. 13. Time history trace showing effective operation of flutter suppression system.

at $k_a = 0$ is divergence. This case introduces new very high frequency flutter boundaries. The correlation between theory and experiment is relatively poor. The following reasons may explain this situation. Theoretically, well-converged boundaries for such high frequency phenomena cannot be expected using even a nine mode analysis because the highest natural frequency of the ninth mode is around 90 cps. Furthermore, the phase shift of the bandpass filter in the feedback loop becomes significant when the frequency is over 10 cps. This effect is not simulated in the theoretical model since a pure gain feedback system is assumed for the sake of simplicity. Experimentally, these high frequency boundaries are very sensitive to the experimental details. For example, a slight misalignment of the gap distances between the permanent magnet and the wire coil can easily result in a relatively large flutter boundary difference.

The low frequency (~1.6 Hz) flutter boundary, which is the most crucial in this problem, is not improved a great deal in these experimental results. By contrast, very high frequency

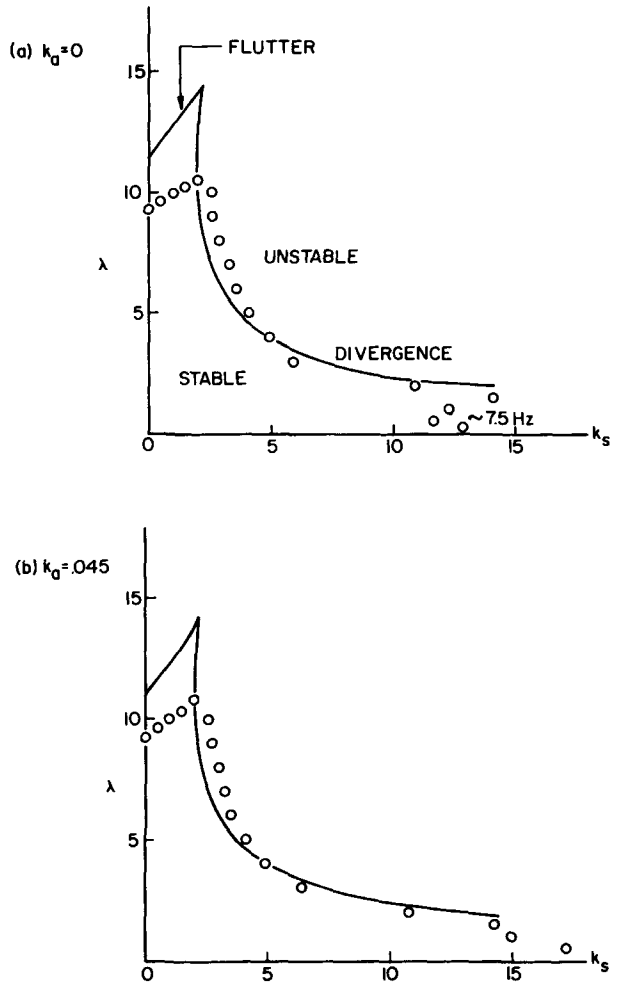

Fig. 14. Stability boundary ($z_{c/L} = 0.9$, $z_{a/L} = 0.95$).

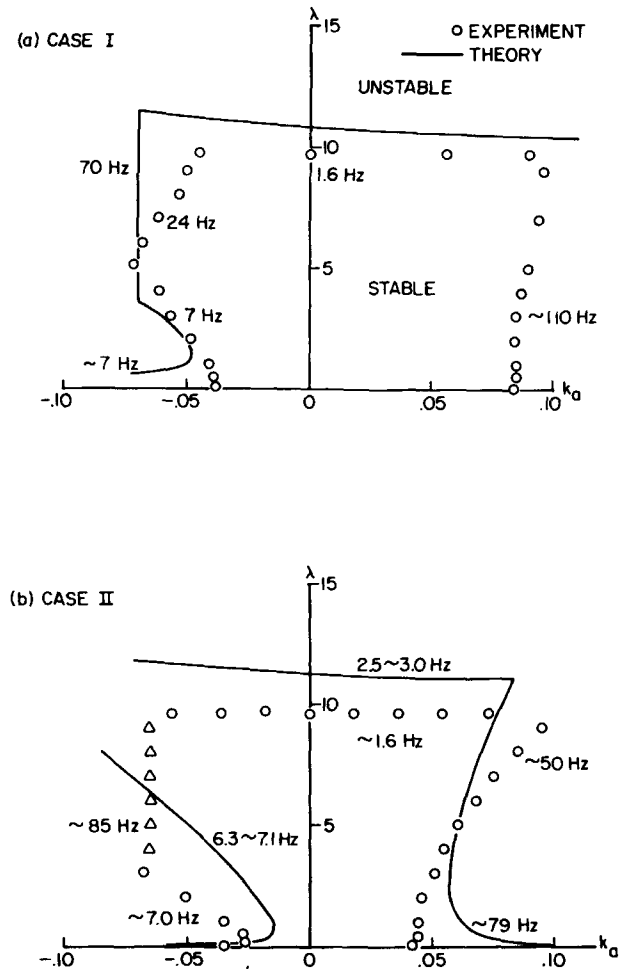

Fig. 15. Stability boundary (torsion acceleration feedback) ($z_{c/L} = 0.3$, $z_{a/L} = 0.45$).

(25 ~ 160 Hz) flutter boundaries have a steep slope. This is due to the nature of acceleration signal that is propertional to the displacement times the square of the frequency of the motion. The flutter boundaries higher than 10 Hz are detected only by the violent diverging oscillation of the feedback electrical signal, but not by the beam motion itself. On the contrary, the boundaries with about 1.6 and 7 Hz can be detected by eye.

(c) *Torsion velocity feedback*

For completeness in the study of systems with a dynamic feedback signal, a torsion velocity feedback system is examined in this section. One representative example for this type of feedback is shown in Fig. 16, where $z_{c/L} = 0.3$, $z_{a/L} = 0.95$. The agreement between theory and experiment is in general good. Three types of stability boundaries exist in the figure. The upper stagility boundary in this figure is limited by a low frequency flutter which is caused by a frequency convergence between the first bending and torsion branches. The left hand side stability boundary, where the torsion velocity feedback gain k_v is negative, is bounded by the loss of damping of the first torsion dominated motion. On the contrary, the right hand side boundary is explained by the loss of damping of the second bending branch.

An experimental maximum increase in the follower force required to cause flutter, by the pure torsion velocity feedback, is about 10% compared to a non-feedback system. Although the pure torsion velocity feedback itself is better than the pure acceleration feedback, this amount is much less than that in the pure torsion strain feedback system. Velocity feedback is one of the intuitive ways to stabilize systems in the sense that damping is added to them. However, in this specific problem, velocity feedback is less effective than the strain feedback as was suggested by the earlier root locus analysis.

3.3.2 *Frequency and damping variation with follower and control forces.* A useful check on our basic understanding of the system is to correlate the results of experiment with theory in as much detail as possible. Experimental data for frequency and damping variation prior to the onset of flutter (subcritical conditions) are rare in the literature and the present data provide an almost unique opportunity for experimental-theoretical correlation. This represents the most

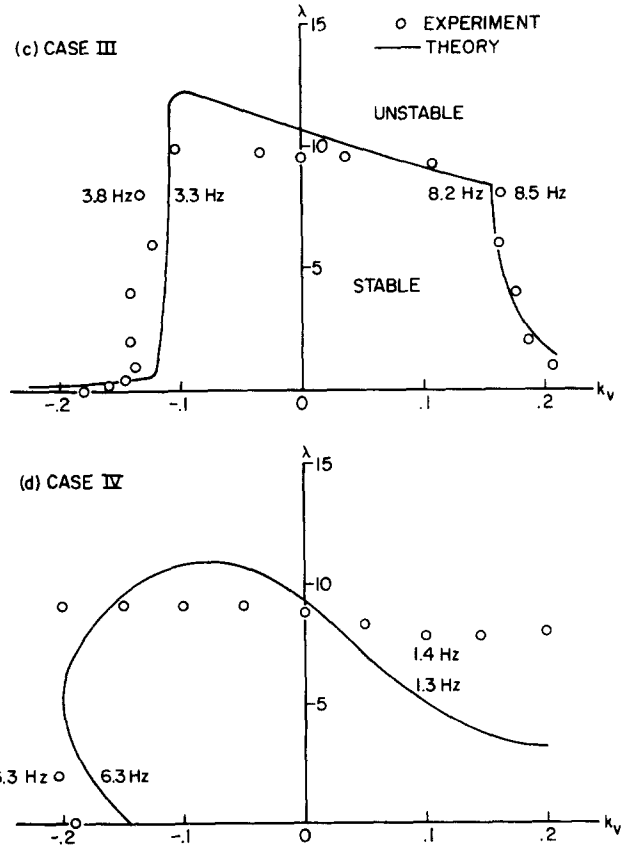

Fig. 16. Stability boundary (torsion velocity feedback) ($z_{c/L} = 0.3$, $z_{a/L} = 0.9$).

complete correlation possible with theory and demonstrates the effectiveness of the flutter suppression system. Most of the experimental data are obtained by a forced response half power method[8]. Sophisticated data reduction techniques such as those discussed in Ref. [3] were not required in the measurement since external excitation was easily applied to this experimental model. Although Ref. [3] measured the damping variation of the least damped mode (i.e. critical mode) in a wind tunnel, the characteristics of the other roots were not recorded experimentally.

(a) *Follower force only*

In Fig. 17, where $z_{c/L} = 0.3$, $z_{a/L} = 0.95$, experimental and theoretical results are given for a beam-follower force system without active feedback. They are presented in the form of root locus plots on the complex s-plane. The correlations are excellent, except for the first bending branch, where the experimental damping data are less accurate[8]. Error bars come from uncertainty in the measurement of the amplitude response to determine the damping ratio.

The first bending and torsion branch frequencies approach each other gradually with increasing follower force. Here the instability of the first bending branch is clearly indicated by its crossing the imaginary axis from negative to positive $Re(s)$. This branch becomes unstable while the damping ratio of the first torsion branch simultaneously increases very rapidly.

(b) *Torsion acceleration and strain feedback*

Figure 18 is for one of the best systems with active feedback control. In this particular case torsion strain gain $k_s = 5.0$ and torsion acceleration feedback gain $k_a = 0.054$ are selected. The first experimental bending mode frequency is seen to decrease steadily with follower force up to a point roughly 35% below critical. Then this frequency begins to increase, while the first torsion branch frequency decreases. This first bending branch frequency decrease with λ (prior to flutter), before eventually increasing, results in about a 40% flutter boundary increase. Theoretical results for frequency variation (Fig. 18) also show the decrease in the first bending mode frequency prior to flutter. Since the addition of the feedback loop increases the possibility of the experimental error, correlation between theory and experiment in these figures is slightly worse than in the case of follower force only. Nevertheless, the general tendency of their

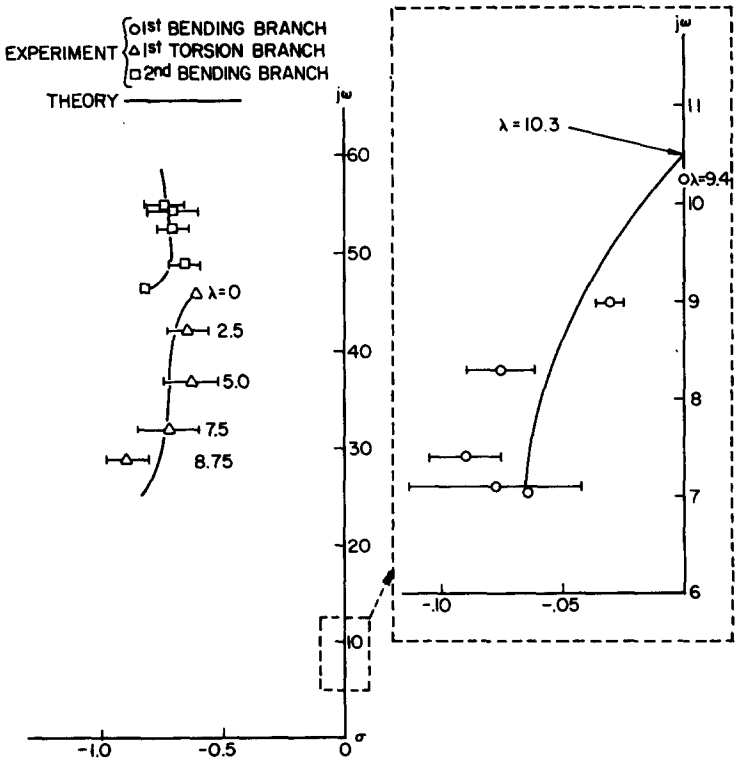

Fig. 17. Root locus with follower force (no active control).

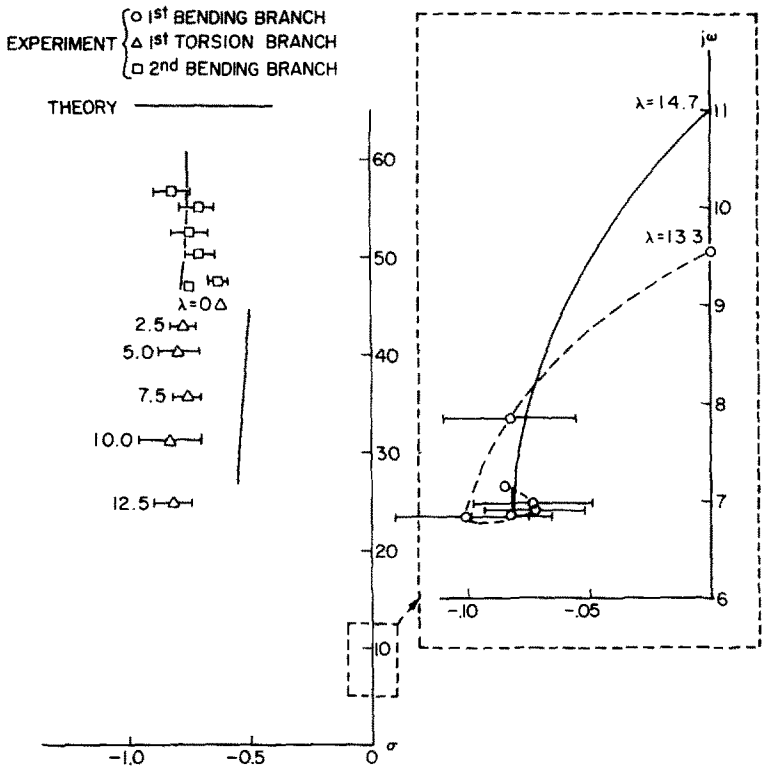

Fig. 18. Root locus with follower force (with active control) ($z_{a/L} = 0.95$, $z_{c/L} = 0.3$, $k_a = 0.054$, $k_s = 5$).

variation is still well-predicted theoretically. In particular, the root locus of the first bending branch in Fig. 18 shows the nature of this feedback system vividly. The introduction of the feedback increases the follower force flutter boundary by 42% experimentally and 44% theoretically.

4. CONCLUSIONS

(1) An increase of follower force required for flutter of over 40% without gain adaptation has been recorded with a combined feedback system of torsion strain and acceleration. This type of instability can be effectively controlled by delaying the frequency convergence between the participating modes. Even order feedback compensations, such as strain or displacement, and acceleration, govern the vertical movement of the characteristic roots along the imaginary axis on the s-plane. Extensive and good correlation between theory and experiment is shown.

The selection of the feedback signal, strain or acceleration, must be made based upon the frequency characteristic of the flutter to be suppressed. For the low frequency boundary, the strain feedback will work effectively. On the other hand, the high frequency flutter will be controlled more easily by the acceleration feedback.

(2) Odd order (velocity) feedback may give only modest improvements or be ineffective in a lightly damped system which exhibits strong converging frequency flutter.

(3) As was indicated in [1], the placement of system zeros, which are the values of the roots when the feedback gain is infinity, is important. These must be placed so that roots exit properly from system poles which are the values of the roots when the gain is zero.

(4) Any active feedback system must be carefully designed in order not to induce new unfavorable instabilities due to its application. A skillful application of both displacement (or strain) and acceleration feedback may give rise to almost independent control of two flutter boundaries with different frequency characteristics.

A parallel study of bending-torsion wing flutter including an experimental wind tunnel investigation is now being undertaken[13].

REFERENCES

1. Supersonic transport flutter SAS conceptual study results. *The Boeing Company Report* D3-7600-9, Wichita Division (1969).

2. Feasibility of an active flutter control demonstration. *The Boeing Company Report D3-8440*, Wichita Division (Dec. 1970).
3. M. C. Sandford, I. Abel and D. L. Gray, Development and demonstration of a flutter suppression system using active controls. *NASA TR R-450* (Dec. 1975).
4. F. C. Moon and E. H. Dowell, The control of flutter instability in a continuous elastic system using feedback. *AIAA/ASME 11th Structures, Structural Dynamics and Matls Conf.* (April 1970).
5. C. F. Kalmbach, Feedback control of flutter instability in a continuous elastic system. *AIAA J.* **10** (1972).
6. C. F. Kalmbach, Active control of an elastic body. Ph.D. Thesis Princeton University, also Department of Aerospace and Mechanical Sciences Report 1036-T (May 1972).
7. C. F. Kalmbach, E. H. Dowell and F. C. Moon, The suppression of a dynamic instability of an elastic body using feedback control. *Int. J. Solids Structures* **10**, 36 (1974).
8. H. Horikawa, Active feedback control of an elastic body subjected to a nonconservative force, Ph.D. Thesis Princeton University, also Department of Aerospace and Mechanical Sciences Report 1331-T (July 1977).
9. S. N. Prasad and G. Herrmann, Stability of a cantilevered bar subjected to a transverse follower force of fluid jet. *Sonder-abdruck aus Ingenieur-Archiv.* 39, *Band* 5 (1970).
10. S. N. Nasser, S. N. Prasad and G. Herrmann, Destabilizing effect of velocity-dependent forces in non-conservative continuous systems. *AIAA J.* **4** (1966).
11. G. Herrmann, Stability of equilibrium of elastic systems subjected to non-conservative forces. *Appl. Mech. Reviews*, **20** (1967).
12. T. M. Yang and G. Herrmann, Feedback control of circulatory elastic systems. *Stanford University Report SUDAM Rep. No.* 72-7 (May 1972).
13. D. E. Dashcund, Development of a theoretical and experimental model for the study of active suppression of wing flutter. Ph.D. Thesis, Princeton University (To be published).
14. R. C. Dorf, *Modern Control Systems*, 2nd Edn. Addison Wesley, New York (1974).
15. E. Nissim, Flutter suppression using active controls based on the concept of aerodynamic energy. *NASA TN D-6199* (March 1971).